J. Fluid Mech. (2007), *vol.* 579, *pp.* 445–466.
doi:10.1017/S0022112007005393 Printed in the United Kingdom

The effects of gravity modulation on fluid mixing. Part 2. Stochastic modulation

V. K. SIDDAVARAM AND G. M. HOMSY

Department of Mechanical Engineering, University of California, Santa Barbara, CA 93106-5070, USA

(Received 31 July 2006 and in revised form 29 November 2006)

We study numerically the effects of zero-mean stochastic gravity modulation on the mixing characteristics of two interdiffusing miscible Boussinesq fluids initially separated by a thin diffusion layer. The gravity modulation has a Gaussian probability distribution and is characterized by an exponentially damped cosine autocorrelation function, i.e. $\langle g(t)g(t+\tau)\rangle/\langle g^2(t)\rangle = \mathrm{e}^{-\lambda\tau}\cos(\omega\tau)$. The associated power spectrum is a Lorentzian with peak at ω and width λ. The flow is found to depend on the following parameters: the Grashof number, Gr, based on the viscous length scale, $l_\nu = \sqrt{\nu/\omega}$; the Schmidt number, Sc; the correlation exponent, λ; and other geometric parameters. Even for extremely small Gr, we observe the propagation of gravity currents, Kelvin–Helmholtz (KH) and Rayleigh–Taylor (RT) instabilities. This is in contrast to the case of harmonic modulation considered in Part 1 (Siddavaram & Homsy *J. Fluid Mech.* vol. 562, 2006, p. 445) wherein these phenomena occur sequentially as Gr increases. The mixed volume is found to vary non-monotonically with the correlation exponent, λ, with narrow-band modulation having the largest mixed volume followed by harmonic modulation and then broadband modulation. This non-monotonicity of the mixed volume with λ is explained on the basis of the competition between the effects of excitation of lower frequencies, which lead to higher mixing, and the effects of the reduction in the energy content at the dominant frequency, which leads to reduced mixing. The value of the correlation coefficient, λ, at which the mixed volume is the largest is found to be independent of Gr. To understand the finer details of the mechanisms, we consider two- and three-frequency modulations. We find that increasing the amplitude of the secondary component when its frequency is smaller than that of the primary component leads to the occurrence of KH and RT instabilities at smaller Gr than that for the case of single-frequency modulation. We have understood the non-monotonic variation in the mixed volume by considering a three-frequency modulation, where one of the frequencies is smaller than the characteristic frequency and the other larger.

1. Introduction

In Part 1 of this paper (Siddavaram & Homsy 2006), we analysed the effects of harmonic gravity modulation on fluid mixing. In this paper, we will focus on the effects of stochastic gravity modulation. Jules *et al.* (2002) found that the microgravity environment, e.g. that aboard the International Space Station (ISS), is characterized by low mean accelerations which are $O(10^{-6})g_e$ (g_e is the gravity on Earth) and fluctuations that are two or three orders of magnitude above the mean, i.e. $O(10^{-4}-10^{-3})g_e$. These gravity fluctuations are collectively termed gravity jitters or g-jitter. Thomson *et al.* (1997) analysed the accelerometer data collected during a NASA mission and

found that the typical acceleration field consists of periodic components, random components with small autocorrelation time, and a white noise background. In order to understand the nature of the flows generated by gravity jitters and to study their effects on fluid mixing, it is therefore essential to consider both deterministic and stochastic models of jitter.

Gresho & Sani (1970) studied the effect of a time-modulated vertical gravity field on the Rayleigh–Bénard instability of a heated fluid layer and concluded that the effect of harmonic gravity modulation is to change the critical Rayleigh number. In particular, a layer of fluid heated from below, which is normally unstable because of the unstable density stratification may be stabilized in certain regions of the amplitude-frequency plane, no matter how large the Rayleigh number is. In contrast, Antar (1977) analysed the effect of small-amplitude random uncorrelated vibrations (white noise) on the stability of a fluid layer heated from below, and concluded that stochastic modulation tends to further destabilize a fluid layer heated from below. Thus the effects of stochastic and deterministic modulations may be qualitatively different.

As noted by Horsthemke & Lefever (1984) and Drolet & Viñals (1997), internal random fluctuations, which are usually of thermal origin, scale inversely with the size of the system and lead to imperfect bifurcations, wherein the bifurcation point is smeared into a small region. These imperfect bifurcations have also been studied by Jhaveri & Homsy (1980) in the context of analysing the onset of Rayleigh–Bénard convection from random thermodynamic fluctuations arising within a fluid. In contrast, the intensity of the externally induced fluctuations (e.g. stochastic forcing or random fluctuations of a parameter), in general, does not scale with the system size and therefore may modify the local stability properties of the system.

Benjamin & Ursell (1954) studied the linear stability of a free surface of a liquid subject to a harmonically varying external force, acting perpendicular to the undeformed surface at rest, and found that the displacement of the surface is governed by Mathieu's equation, with potential for parametric resonance, and that the free-surface response was subharmonic. Zhang, Casademunt & Viñals (1993) analysed the same problem when the external force is stochastic. In the underdamped limit, this problem reduces to a study of the parametric harmonic oscillator for each of the Fourier modes of the surface displacement. They observed parametric resonance in a wide frequency range when the external force had a broad frequency spectrum. The above results are similar to those observed in the case of harmonic modulation. However, they found that the resonant behaviour in the case of stochastic modulation is, in general, weaker than that which results from an equivalent monochromatic modulation. They defined the stability of the solutions on the basis of time-dependence of second-order moments, which are related to the average energy of the oscillations, and obtained neutral stability curves in the limit of low frequencies and near resonance. They also studied the effects of varying the width of the noise spectrum on the stability and found that when the forcing is broadband, increasing the correlation time leads to an increase in the stability, whereas when the forcing is monochromatic, increasing the correlation time leads to a decrease in stability.

Thomson, Casademunt & Viñals (1995) studied the effects of a stochastically varying gravity field on the flow inside a laterally heated cavity. The acceleration is perpendicular to the initial density gradient and the heat transfer is conduction dominated. When the modulation is periodic, they find that the vorticity field is oscillatory with a zero mean and has a root-mean-squared (r.m.s.) value that is proportional to the Rayleigh number, and even in the absence of viscous dissipation, the r.m.s. value

remains bounded. When the modulation is stochastic, the mean value of the vorticity field is zero. However, the r.m.s. value grows linearly with time, until it saturates owing to viscous diffusion.

Drolet & Viñals (1997) studied the effect of stochastic modulation on a system with $O(2)$ symmetry that exhibits Hopf bifurcation in the absence of modulation. The study included a random component in both the control parameter of the bifurcation and the modulation amplitude. At a Hopf bifurcation in a periodically modulated system, the trivial state loses stability to either travelling waves when the modulation amplitude is small, or standing waves when the amplitude is sufficiently large. They concluded that when the modulation amplitude has a stochastic component, the threshold for the onset of instability in the standing-wave regime is shifted from its deterministic location and the region of primary bifurcation to travelling waves disappears. The main conclusion from all of the above studies is that the effects of stochastic modulation may be qualitatively different from those of harmonic modulation.

Duval & Jacqmin (1990) studied the effects of zero-mean harmonic gravity modulation on two interdiffusing miscible fluids separated by a vertical diffusion layer. They identified two types of instability: Kelvin–Helmholtz instability associated with the growth and oscillation of the interface, and 'chaotic instability' associated with the breakup of the interface. They proposed that the initial breakup of the interface occurs by means of Rayleigh–Taylor instability. The analysis of Duval & Jacqmin (1990) was extended in Part 1 of this paper and the parameters were varied over a wider range. We found that the solution depended on the following parameters: the Grashof number, Gr, based on the viscous length scale and buoyancy velocity; the Schmidt number, Sc; the phase angle of the modulation; and geometric parameters. We observed the following flow regimes as Gr was increased: (i) neutral oscillations at the forcing frequency; (ii) successive folds which propagate diffusively; (iii) Kelvin–Helmholtz (KH) instabilities on the folds leading to interfacial breakup and; (iv) both KH and Rayleigh–Taylor (RT) instabilities, leading to rapid mixing. By varying Sc, we determined that the mechanism for the formation of the instabilities was inertial in nature, hence the critical Gr for the onset of KH and RT instabilities, $Gr_{c,KH}$ and $Gr_{c,RT}$, respectively, are independent of Sc for moderate to large Sc.

In this paper, we will examine the effects of stochastic vertical gravity modulation on the mixing characteristics of two interdiffusing miscible fluids separated by a thin vertical diffusion layer. We will consider both narrow-band (coloured noise) and broadband (white noise) stochastic modulation. Our main objective is to compare the flow regimes and instabilities obtained for stochastic gravity modulation with those obtained for harmonic modulation. We ask if the flow instabilities that are observed in the case of stochastic modulation are the same as those observed for harmonic modulation and if stochastic modulation leads to the same well-defined smooth progression of the flow regimes with increasing Gr as observed in the case of harmonic modulation. We will also compare the mixed volumes (to be defined later) obtained in both forms of modulation and explain the differences.

2. Problem formulation

Since we are mainly interested in a qualitative description of the mixing mechanisms and instabilities, we focus our attention on two-dimensional effects and assume that gravity is entirely in the vertical direction. Figure 1(a) shows a schematic of the model problem. The following equations governing the evolution of the non-dimensionalized

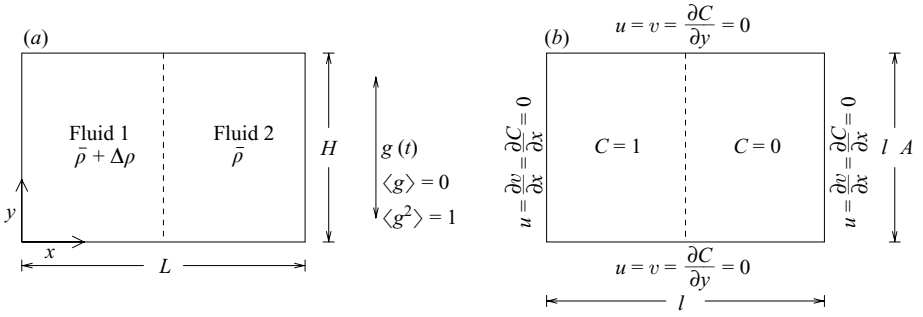

FIGURE 1. Schematic of (*a*) the two-dimensional problem (*b*) the initial and boundary conditions in dimensionless terms.

flow and concentration fields have been given in Part 1.

$$\frac{\partial u}{\partial x} + \frac{\partial v}{\partial y} = 0, \tag{2.1}$$

$$\frac{\partial u}{\partial t} + Gr\left(u\frac{\partial u}{\partial x} + v\frac{\partial u}{\partial y}\right) = -Gr\frac{\partial p}{\partial x} + \left(\frac{\partial^2 u}{\partial x^2} + \frac{\partial^2 u}{\partial y^2}\right), \tag{2.2}$$

$$\frac{\partial v}{\partial t} + Gr\left(u\frac{\partial v}{\partial x} + v\frac{\partial v}{\partial y}\right) = -Gr\frac{\partial p}{\partial y} + \left(\frac{\partial^2 v}{\partial x^2} + \frac{\partial^2 v}{\partial y^2}\right) + g(t), \tag{2.3}$$

$$\frac{\partial C}{\partial t} + Gr\left(u\frac{\partial C}{\partial x} + v\frac{\partial C}{\partial y}\right) = \frac{1}{Sc}\left(\frac{\partial^2 C}{\partial x^2} + \frac{\partial^2 C}{\partial y^2}\right). \tag{2.4}$$

In (2.1)–(2.4) $g(t)$ is the non-dimensional gravity which is normalized such that its standard deviation, g, is 1. We consider stochastic gravity modulations that have zero mean, are characterized by an exponentially damped cosine autocorrelation function, i.e. $\langle g(t)g(t+\tau)\rangle = \mathrm{e}^{-\lambda\tau}\cos(\omega\tau)$, and whose probability distribution function is Gaussian. Modulations having the above statistics have also been used by Thomson *et al.* (1995) and Zhang *et al.* (1993). The one-sided power spectrum associated with the jitter is a Lorentzian with width λ and has a single well-defined peak at ω, which is chosen as the characteristic frequency. We measure time in units of 'periods', where 1 period $= 2\pi/\omega$, so in non-dimensional terms, the autocorrelation of gravity is $\mathrm{e}^{-\lambda\tau}\cos(\tau)$. Also, note that when the correlation coefficient $\lambda = 0$, the modulation reduces to monochromatic noise, which will allow us to validate our results with those for harmonic modulation discussed in Part 1. More will be said about this later. When $\lambda \to \infty$ and $\omega = 0$, the modulation is equivalent to white noise. Thus, varying λ offers us an easy way of smoothly changing the modulation from monochromatic noise to broadband white noise. Since gravity jitters are characterized by low mean and large fluctuations, it is reasonable to assume that the mean gravity is zero. Finally, Thomson *et al.* (1997) analysed the actual accelerometer data collected during a microgravity mission and found that the probability distribution function associated with the jitter is Gaussian for small amplitudes.

All the other variables are scaled in the same way as described in Part 1. We define our characteristic time scale as the reciprocal of ω. The length scale is chosen as the viscous length, $l_\nu = \sqrt{\nu/\omega}$, where $\nu = \mu/\bar{\rho}$ is the kinematic viscosity. The velocity scale is chosen as the buoyancy velocity, $U_c = (\Delta\rho/\bar{\rho})(g/\omega)$. In the above equations, $Gr = U_c/\omega l_\nu = (\Delta\rho/\bar{\rho})(g/\nu^{1/2}\omega^{3/2}) = (\Delta\rho/\bar{\rho})g(l_\nu^3/\nu^2)$ is a Grashof number, $Sc = \nu/D$ is the Schmidt number. Note that there is a slight difference in the definition of Gr

adopted here and that used in Part 1. For the case of stochastic modulation, the Gr is based on the standard deviation of the modulation, g, whereas in SH, Gr is based on the amplitude of the harmonic gravity modulation, which is $\sqrt{2}$ times the standard deviation.

The relevant parameters governing the two-dimensional problem are then the Grashof number, $Gr = (\Delta\rho/\bar{\rho})(g/\omega^{3/2}\nu^{1/2})$; the Schmidt number, $Sc = \nu/D$; the exponential coefficient of autocorrelation, λ; the non-dimensional length of the domain, $l = L/l_\nu$; and the aspect ratio of the domain, $A = H/L$ where H and L are the height and length of the domain, respectively. The last two parameters are introduced through the boundary conditions which will be discussed later.

Equations (2.1)–(2.4) are now recast into streamfunction–vorticity formulation as in Part 1. The equations become

$$\frac{\partial^2\psi}{\partial x^2} + \frac{\partial^2\psi}{\partial y^2} = -\xi, \tag{2.5}$$

$$\frac{\partial\xi}{\partial t} + Gr\left(u\frac{\partial\xi}{\partial x} + v\frac{\partial\xi}{\partial y}\right) = \left(\frac{\partial^2\xi}{\partial x^2} + \frac{\partial^2\xi}{\partial y^2}\right) + \left(\frac{\partial C}{\partial x}\right)g(t), \tag{2.6}$$

$$\frac{\partial C}{\partial t} + Gr\left(u\frac{\partial C}{\partial x} + v\frac{\partial C}{\partial y}\right) = \frac{1}{Sc}\left(\frac{\partial^2 C}{\partial x^2} + \frac{\partial^2 C}{\partial y^2}\right). \tag{2.7}$$

Also as in Part 1, we choose the following initial condition for the concentration, C:

$$t = 0: \quad C = \tfrac{1}{2}\,\mathrm{erfc}\left(\frac{x - 0.5l}{\delta}\right). \tag{2.8}$$

Note that the above initial condition introduces an additional parameter into the problem: δ, the steepness of the initial concentration profile. It has been found in many similar problems that the dependence on δ is very slight.

We assume that the fluids are initially at rest. Therefore

$$t = 0: \quad \xi = 0, \quad \psi = 0. \tag{2.9}$$

The boundary conditions are as follows:

$$x = 0, l: \quad u = \frac{\partial v}{\partial x} = \frac{\partial C}{\partial x} = 0. \tag{2.10}$$

The above equation corresponds to the boundary conditions of no fluid penetration, no shear stress, and no mass flux along the vertical walls.

$$y = 0, lA: \quad u = v = \frac{\partial C}{\partial y} = 0. \tag{2.11}$$

Equation (2.11) corresponds to the boundary conditions of no fluid penetration, no slip, and no mass flux along the horizontal walls. We will be solving (2.5)–(2.7), subject to (2.8)–(2.11). Figure 1(*b*) shows a sketch of the domain along with the boundary conditions.

We use the pseudospectral algorithm described in Part 1 to solve the above equations subject to the initial and boundary conditions. Spectral methods are used in the x-direction and compact finite differences, which are fourth-order in the interior and third-order at the boundaries, are used in the y-direction. The time-stepping is done through operator splitting in which all terms except the stochastic one are advanced by a classical fourth-order explicit Runge–Kutta scheme. In order to compute the

Position	$\xi_{stochastic}$	$\xi_{harmonic}$	$C_{stochastic}$	$C_{harmonic}$
$x = 269.53125, \quad y = 1.5625$	−0.017237	−0.017411	1	1
$x = 476.4625, \quad y = 64.0625$	−0.001573	−0.001478	0.545523	0.54426

TABLE 1. Validation of stochastic modulation for $\lambda = 10^{-4}$ with harmonic modulation.

integral of the stochastic gravity term, we use the algorithm provided in the Appendix of Thomson *et al.* (1995).

In order to understand the evolution of the field variables in the mean, we compute the ensemble averages which are obtained by first computing the field variable in question (concentration say) for each individual gravity realization, and then averaging the field variable over a fairly large number of realizations of $g(t)$. We increase the number of realizations in increments of 10 until the results obtained with successive numbers of realizations are within 5% of each other. For the parameter ranges considered here averaging over 40 realizations was enough to achieve this level of accuracy and unless otherwise specified, the results are reported for 40 realizations.

For validation, we compared our results for correlated stochastic modulation when the correlation coefficient $\lambda \to 0$, with the results for harmonic modulation presented in Part 1. When $\lambda = 0$, the autocorrelation for correlated stochastic modulation is $\cos(t)$ which is the same as the autocorrelation in the case of harmonic modulation wherein the gravity varies as $\sqrt{2}\cos(t+\phi)$. Thus, for small values of λ, we expect the ensemble-averaged flow and concentration variables for correlated stochastic modulation for a given Gr to be the same as the phase-averaged flow and concentration variables in the case of harmonic modulation corresponding to $\sqrt{2}Gr$. The phase-averaged field variables for the case of harmonic modulation are computed by averaging the field variable in question over the different individual harmonic gravity realizations for different values of the phase angle, ϕ, which is varied from 0 to 2π. In table 1, we show the excellent agreement between the vorticity and concentration values for $Gr = 7$ and $\lambda = 10^{-4}$ ($Gr = 7\sqrt{2}$ for the harmonic case) after 10 time periods for the cases of harmonic and stochastic formulations. To illustrate the agreement, we plot the ensemble-averaged and phase-averaged concentration fields (figure 2). For clarity, we show only the contours depicting concentration values between 0.25 and 0.75. The slight asymmetry that we see in the case of stochastic modulation is due to sampling errors.

3. Results

The reference values of the six parameters governing the problem are as follows. We fix $Sc = 1$, which corresponds to the case of mixing of gases, and $A = 0.2$ which means that the domain is a horizontal slender cavity. l is fixed at 1000, resulting in a reasonably large domain (a thousand viscous lengths, l_v) so that the evolution of the interface is free from any end effects over a reasonably long time. δ is set at 10, resulting in a reasonably sharp but continuous interface and the correlation coefficient λ is initially fixed at 1.0, which corresponds to the case of narrow-band gravity modulation. Gr was varied from 1 to 15 (resulting in Grashof numbers based on the length of the domain ($Gr_L = Gr\,l^3$) of the order of 10^{10}). Various quantities, especially the interfacial evolution, were studied as a function of time. Note that time is measured in 'periods', which are defined on the basis of the characteristic frequency identified in § 2. Also, unless otherwise specified, whenever we plot the concentration

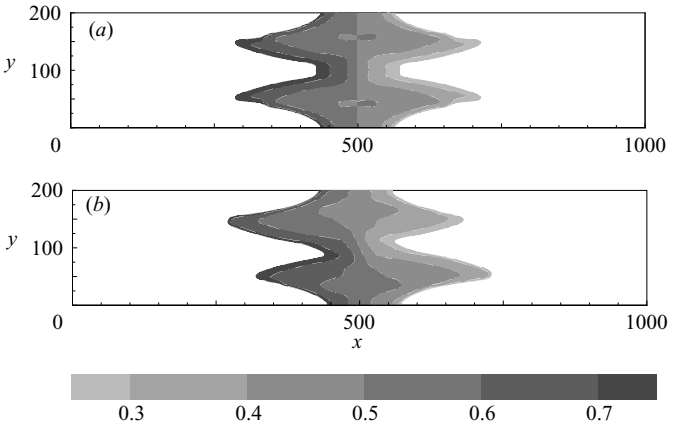

FIGURE 2. Validation of the results for $Gr = 7$ and after 10 periods. (*a*) Phase-averaged concentration field for harmonic modulation (cf. Part 1). (*b*) Ensemble-averaged concentration field for stochastic modulation with $\lambda = 10^{-4}$.

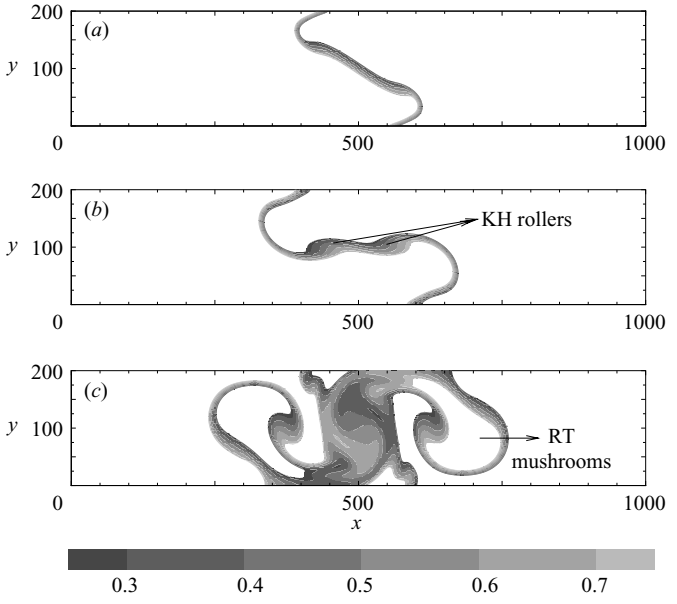

FIGURE 3. Concentration fields for $Gr = 0.3$. (*a*) Gravity current at $t = 15$ periods. (*b*) KH instability at $t = 25$ periods. (*c*) RT instability at $t = 60$ periods.

field, we show only the contours depicting the concentration values between 0.25 and 0.75, even though the full range of the concentration values extends from 0 to 1.

3.1. *Effect of Gr*

The individual realizations of the flow and concentration fields naturally depend on the individual realizations of $g(t)$. In figure 3, we show the concentration fields for a typical realization at three different times for a very small $Gr = 0.3$. For small times (figure 3*a*), we observe the propagation of a gravity current similar in appearance to that observed in the case of harmonic modulation with non-zero phase angle albeit at higher Gr (cf. figure 26*a* of Part 1).

The front of this gravity current demarcates the two regions where the velocities of the heavy and the lighter fluids are of opposite sign, thus setting up a velocity gradient. Thus, at later times, there is a potential for shear instabilities, such as those observed in Part 1, figure 26(*b*). The rollers due to KH instability occurring on the gravity current can be seen in figure 3(*b*). There are also regions in the domain where the net acceleration is directed from the lighter fluid towards the heavy fluid, creating the potential for RT instability. Also, the rollers associated with KH instability act as a stirring mechanism, placing packets of heavy fluid above lighter fluids, thus enhancing the potential for RT instability. The mushroom structures associated with RT instabilities can be seen in figure 3(*c*).

We now discuss the reason for the formation of this gravity current. Suppose the gravity is initially negative (pointing downward). As a result, the heavier fluid which is on the left-hand side of the cavity starts flowing to the right along the bottom of the cavity and the lighter fluid flows to the left along the top. When the gravity vector changes direction, the heavier fluid does not immediately return to its initial position, but continues moving to the right, because of finite fluid inertia at finite *Gr*. Eventually, depending upon the initial magnitude of the gravity and the time over which the gravity remains of the same sign, the gravity current reverses its direction or continues coasting in the same direction. We have noticed several instances in which the eventual direction of coasting of the gravity current is opposite to the initial direction of propagation of the current. However, this reversal in direction happens only during the very early stages ($t < 5$ periods).

Although the occurrence of these gravity currents, KH instabilities and RT instabilities, is similar to what we observe in the case of harmonic modulation with non-zero phase angle, the *Gr* at which the instabilities first occur are much lower than in the case of harmonic modulation (for which $Gr_{c,KH} = 12$ and $Gr_{c,RT} = 18$). On the contrary, for stochastic modulation, we have observed that KH and RT instabilities always occur no matter how small *Gr* is. Thus, there is no critical *Gr* for the occurrence of KH and RT instabilities in the case of stochastic modulation. The reason for the occurrence of these instabilities at smaller values of *Gr* in the case of stochastic modulation is as follows. For stochastic modulation, any realization of $g(t)$ is expected to contain instantaneous gravity values that are much larger than the standard deviation on which *Gr* is based. These rare but important events are instrumental in causing KH and RT instabilities.

As *Gr* is increased, the magnitude of the velocity gradient, set up by the gravity current, increases, resulting in an increased potential for KH instability at higher *Gr*. Also, an increasing *Gr* corresponds to larger density difference, higher acceleration, sharper density gradients, or all three, thus causing an increased potential for RT instability. Hence for higher *Gr*, we expect both KH and RT instabilities to occur at earlier times. This is what we observe in figure 4 wherein we show the concentration fields at $t = 14.5$ periods, for the same individual gravity realization, for $Gr = 0.3, 1.5, 4, 7$ and 10. This particular gravity realization was chosen because it leads to easily identifiable KH and RT instabilities (cf. figure 4*b*); however, this behaviour has been observed for other realizations of $g(t)$.

In figure 5, we compare the ensemble-averaged concentration fields at $t = 6$ periods for $Gr = 3, 7, 10$ and 13. We observe the occurrence of a symmetric structure in the middle of the domain which is similar in appearance to that formed for phase-averaged harmonic modulation (cf. figure 27 of Part 1). At any given time, the spread of this structure is larger for higher *Gr* suggesting that mixing is faster for higher *Gr*. In order to quantify the amount of mixing, we use the fractional mixed

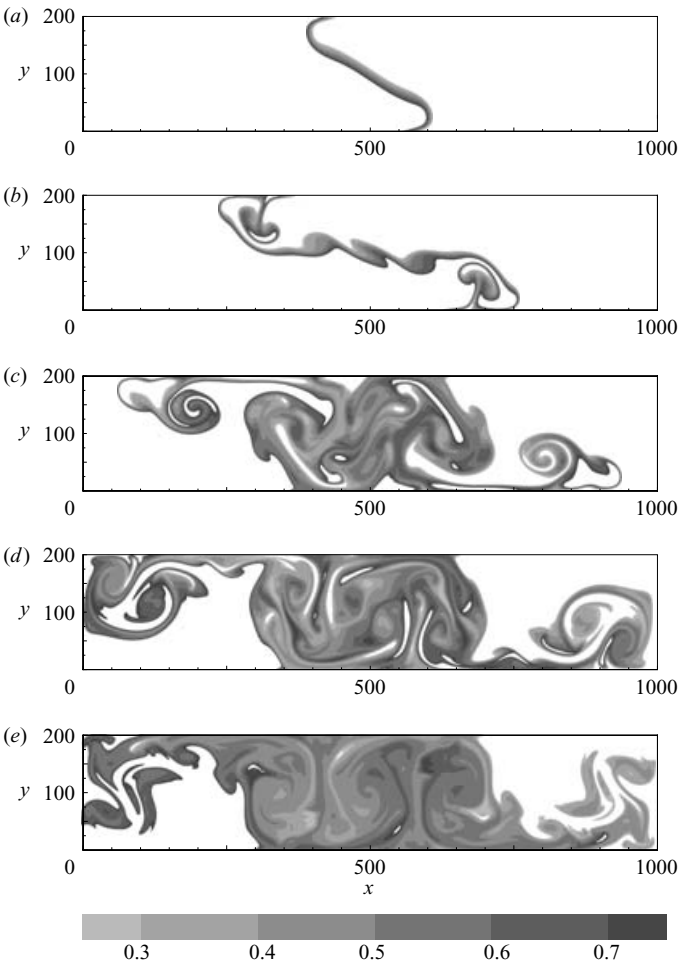

FIGURE 4. Concentration fields at $t = 14.5$ periods for (*a*) $Gr = 0.3$ – gravity current, (*b*) $Gr = 1.5$ – KH + RT, (*c*) $Gr = 4.0$ – disordered concentration field, (*d*) $Gr = 7.0$ – disordered concentration field (RT mushrooms are visible), (*e*) $Gr = 10.0$ – disordered concentration field.

volume, V_m, defined as the fractional volume over which the non-dimensionalized concentration values lie between 0.3 and 0.7. (This definition of V_m is slightly different from that adopted in Part 1, wherein we measure the fractional volume over which the concentration lies between 0.45 and 0.55. However, this change does not affect the trends in the mixed volume variation, which are our primary concern.) In figure 6, we plot the fractional mixed volumes of the ensemble averages *vs.* time for various *Gr*. As expected, mixed volume increases with time and is larger for larger *Gr*. This is because the flow becomes more disordered as *Gr* is increased.

Also as expected, the individual realizations corresponding to different gravity realizations exhibit different amounts of mixing. In figure 7, we show individual realizations of the concentration fields corresponding to the cases of very high mixing and very low mixing at a given time. As can be seen, the realization exhibiting high mixing, whose fractional mixed volume after 10 periods is 0.57, is characterized by the presence of a large roller wave, whose significance will be discussed shortly. This roller is absent in the realization exhibiting low mixing, whose fractional mixed volume at

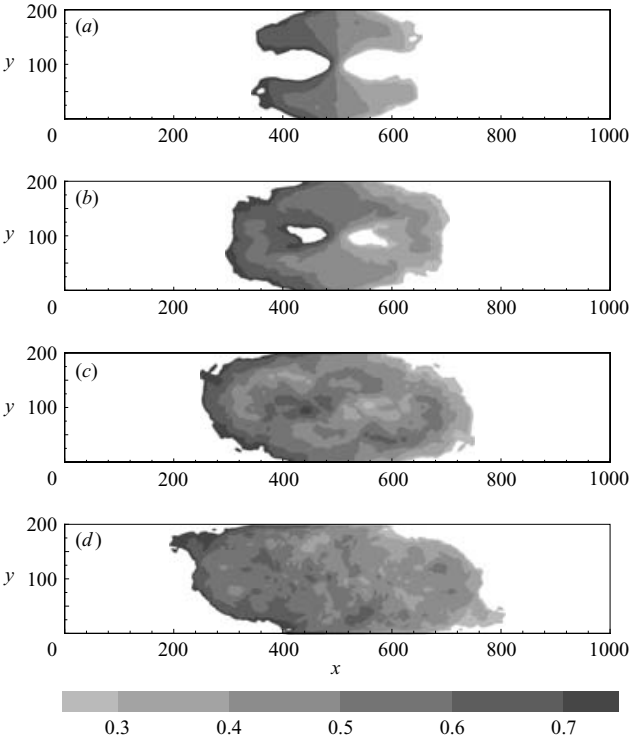

FIGURE 5. Ensemble-averaged concentration fields at $t = 6$ periods, with $\lambda = 1$ for (*a*) $Gr = 4$, (*b*) $Gr = 7$, (*c*) $Gr = 10$, (*d*) $Gr = 13$.

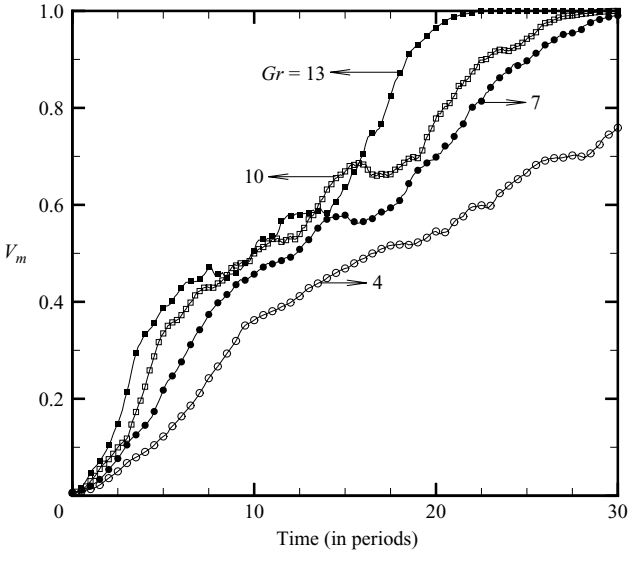

FIGURE 6. Mixed volume *vs.* *Gr* for $Gr = 4, 7, 10$ and 13.

the same time is only 0.20. We have observed that all the realizations that exhibit high mixing are characterized by the presence of large rollers in the concentration field. These are approximately the size of the height of the domain, and are formed

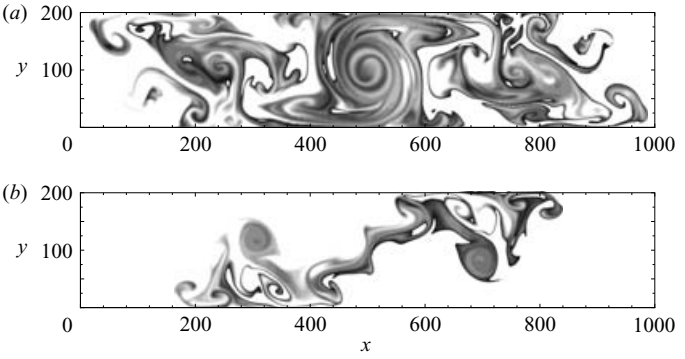

FIGURE 7. Individual realizations for $Gr = 13$ at $t = 10$ periods. (a) High mixing, mixed volume = 0.57 and (b) Low mixing, mixed volume = 0.20.

at the centre of the domain by the pairing of two smaller rollers that appear on the mixing front. The large roller then serves as a stirring mechanism bringing packets of heavy fluid above the lighter fluid, thus exciting Rayleigh–Taylor instabilities and enhancing mixing.

Vortex pairing is an important mechanism of turbulent mixing-layer growth. Winant & Browand (1974) found that unstable waves resulting from Kelvin–Helmboltz instability grow and the fluid rolls up into discrete two-dimensional vortices, which then interact by rotating around each other, forming a single vortex. As illustrated by Meunier, Le Dizès & Leweke (2005) and Cerretelli & Williamson (2003), the vortex merging process is characterized by four stages. In stage I, the vortices rotate around each other and the core size of the vortices increases by viscous diffusion. In stage II, the vortex pair merges, the vortices are deformed and the vortex filaments are generated at the extremities of the pair. However, at the end of this stage, the vortex separation does not reduce to zero, and there are two separate maxima of vorticity. In stage III, the vortex separation ultimately vanishes owing to viscous diffusion and the merged vortex, which is elliptical, becomes axisymmetric. In stage IV, the merged vortex diffuses and its core size grows.

These same processes are seen in our simulations. The merging of two smaller KH rollers to form a larger one and the growth of the resulting vortex with time are shown in figures 8 and 9, wherein the various phases described above are identified in the figure captions. Thus, stochastic jitter results in dynamics that are similar to those at play in free shear layers.

3.2. *Effect of* λ

As detailed in § 2, λ is a measure of the duration over which the gravity is correlated and is also related to the time over which gravity is of the same sign. Increasing λ corresponds to increasing the width of the power spectrum associated with gravity, with $\lambda = 0$ corresponding to harmonic (or monochromatic) modulation, moderate values of λ corresponding to narrow-band stochastic gravity modulation (or coloured noise), and large values of λ corresponding to broadband stochastic gravity modulation (or white noise). The effect of varying λ is shown in figure 10, in which we plot the ensemble-averaged concentration fields for harmonic modulation and representative cases of narrow-band modulation and broadband modulation. Mixed volume, represented by the extent of the dispersive structure, is the largest for narrow-band modulation. In figure 11, we plot the fractional mixed volume with time for

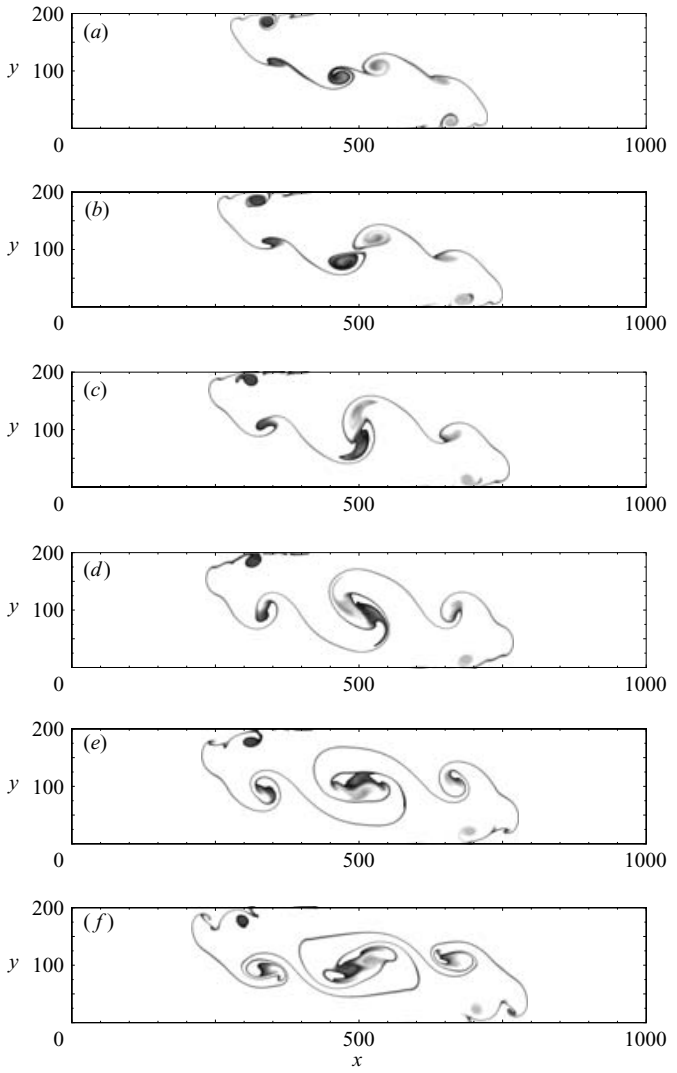

FIGURE 8. Vortex merging for $Gr = 13$ after (*a*) $t = 2.75$ periods – phase I, (*b*) $t = 3.00$ periods – phase I, (*c*) $t = 3.25$ periods – phase II, (*d*) $t = 3.50$ periods – phase II, (*e*) $t = 3.75$ periods – phase II and (*f*) $t = 4.00$ periods – phase II.

$Gr = 7$ for different values of λ. Again as expected, the fractional mixed volume increases with time. However, we note that there is a non-monotonic dependence of the mixed volume on λ. This is illustrated better in figure 12 wherein we plot the fractional mixed volume after 30 periods as a function of λ. As can be seen, mixed volume at any given time is the largest for narrow-band modulation followed by harmonic modulation and then broadband modulation. We also note that the value of λ at which the mixed volume is the largest, denoted as λ_{max}, is constant across a wide range of Gr. This is shown in figure 13 where we plot the mixed volume at $t = 20$ periods with λ for $Gr = 4, 7, 10$ and 13. The value of λ_{max} is 1.05.

The reason for the non-monotonic behaviour of mixed volume with λ is explained as follows. As λ is increased, the width of the power spectrum associated with the

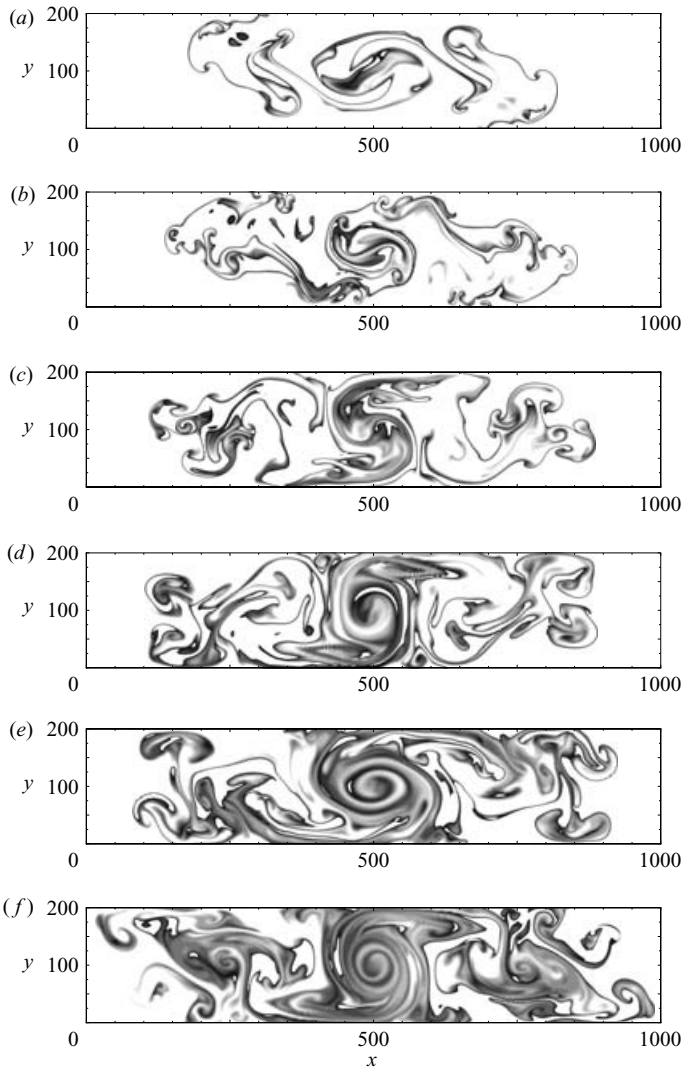

FIGURE 9. Growth in the size of the central vortex for $Gr = 13$ after (*a*) $t = 5$ periods – phase II, (*b*) $t = 6$ periods – phase II, (*c*) $t = 7$ periods – phase II, (*d*) $t = 8$ periods – phase III, (*e*) $t = 9$ periods and – phase III, (*f*) $t = 10$ periods – phase IV.

gravity increases, which means that the gravity modulation now contains a band of frequencies. Also, because the variance of the modulation is held constant, the area under the power spectrum curve is constant and therefore the height of the power spectrum decreases as its width increases. This means that increasing λ at a fixed Gr corresponds to exciting the system at a range of frequencies at the expense of reducing the amount of energy contained in the dominant frequency. It was shown in Part 1 that lower frequency modulation tends to make the concentration and flow fields more disordered. Thus, if we increase the width of the power spectrum, keeping the energy contained in the dominant frequency the same, we expect the mixed volume to increase. It was also shown in Part 1 that, reducing Gr (which is related to the energy contained in the dominant frequency) decreases the disorder and hence the mixed volume. Hence,

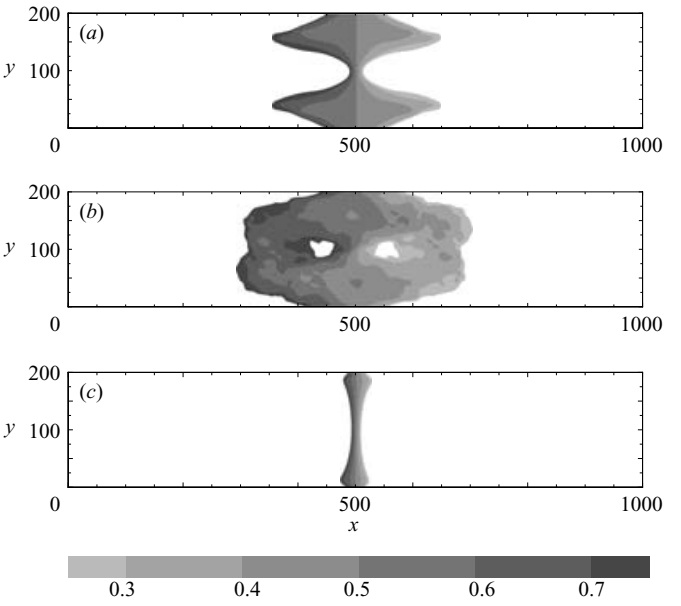

FIGURE 10. Ensemble-averaged concentration fields at $t = 6$ periods and $Gr = 7$ for (a) monochromatic modulation, $\lambda = 0$, (b) narrow-band modulation, $\lambda = 0.53$, (c) white-noise modulation, $\lambda = 5300$.

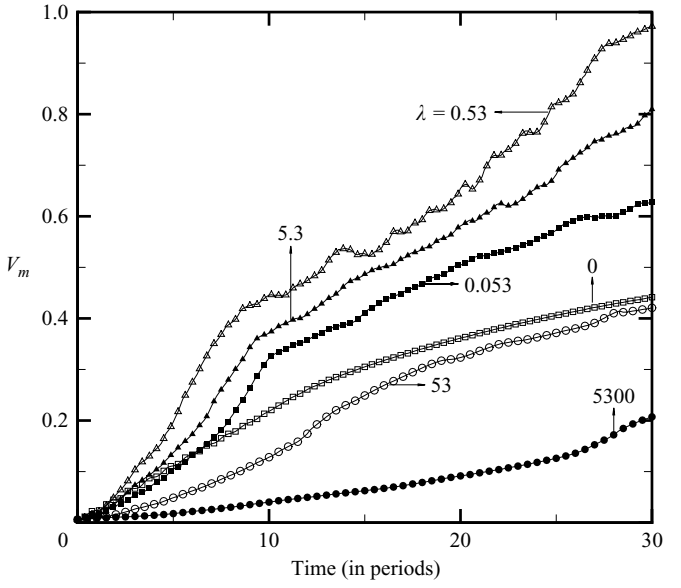

FIGURE 11. The increase in the mixed volume with time for various λ for $Gr = 7$.

decreasing the energy content in the dominant frequency, while keeping the width of the power spectrum constant, reduces the mixed volume. Therefore, for small to moderate values of λ, increasing λ leads to increasingly disordered concentration and flow fields, because the attendant decrease in the energy content at the dominant

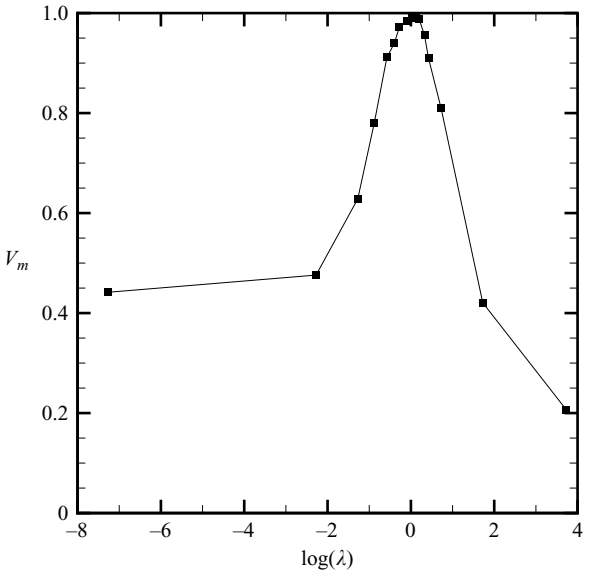

FIGURE 12. The non-monotonic dependence of the mixed volume with λ for $Gr = 7$ and after $t = 30$ periods.

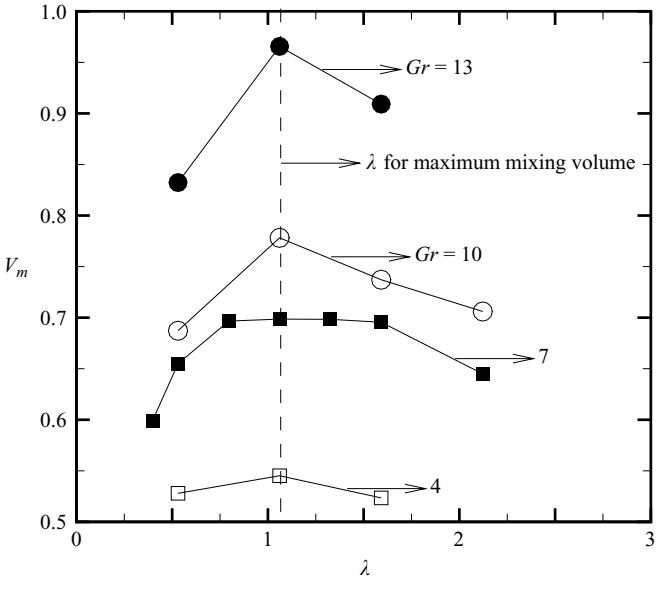

FIGURE 13. The constancy of the λ at which the largest mixed volume occurs with Gr. $\lambda_{max} = 1.05$.

frequency is not significantly large. However, for large values of λ, the amount of energy contained in the dominant frequency is very small. So any increase in the mixed volume owing to the excitation of smaller frequencies is more than offset by the reduction in the mixed volume owing to this decreasing energy content. So for large λ, increasing λ leads to a decrease in the mixed volume. This leads to a non-monotonic variation of the mixed volume as λ is increased from small to large values.

4. Multiple frequency modulation

As explained in earlier sections, stochastic modulation with a non-zero λ corresponds to exciting the system at a band of frequencies whose width is related to λ. Even though the analysis carried out above has given us considerable insight into the problem, in order to understand the finer details of the mechanism, and also to validate the hypothesis presented in the preceding paragraph, we simplify the forcing considerably to include only a finite number of frequencies. We explain some of the results observed in the case of stochastic modulation based on our understanding of the results obtained for this relatively simpler $g(t)$.

We take the following form for the gravity modulation:

$$g(t) = a(\cos(\omega t + \phi) + \epsilon \cos(r\omega t + \phi)).$$

We choose ω as our characteristic frequency and $T = 1/\omega$ as the characteristic time scale. We will refer to the component with frequency ω as the primary component and the one with frequency $r\omega$ as the secondary component. The parameter ϵ is varied between 0 and 100, so that the magnitude of the secondary component may be smaller or larger than that of the primary component. Gravity is normalized by g, which is defined on the basis of an 'equivalent amplitude' as

$$g = \sqrt{2 \int_0^{T^*} \frac{1}{T^*} \left[g(t) - \frac{1}{T^*} \int_0^{T^*} g(t)\, \mathrm{d}t \right]^2 \mathrm{d}t}. \tag{4.1}$$

In the above equation, T^* is the final time until which we would like to observe the evolution of the interface, and is measured in terms of the number of periods based on the characteristic frequency. We compute the standard deviation of $g(t)$ over the times $[0: T^*]$ and multiply it by $\sqrt{2}$ to obtain the equivalent amplitude (note that for a single frequency modulation, this amplitude is $\sqrt{2}$ times the standard deviation). There are two main advantages to defining g in this way. First, when $\epsilon = 0$, i.e. for single-frequency modulation, g reduces to the amplitude of the modulation a. Secondly, the above definition is general enough to be valid for irrational values of r (quasi-periodic modulation). The following equations describe the flow and concentration fields:

$$\frac{\partial^2 \psi}{\partial x^2} + \frac{\partial^2 \psi}{\partial y^2} = -\xi, \tag{4.2}$$

$$\frac{\partial \xi}{\partial t} + Gr\left(u\frac{\partial \xi}{\partial x} + v\frac{\partial \xi}{\partial y}\right) = \left(\frac{\partial^2 \xi}{\partial x^2} + \frac{\partial^2 \xi}{\partial y^2}\right) + \left(\frac{\partial C}{\partial x}\right)\frac{a(\cos(\omega t) + \epsilon \cos(r\omega t))}{g}, \tag{4.3}$$

$$\frac{\partial C}{\partial t} + Gr\left(u\frac{\partial C}{\partial x} + v\frac{\partial C}{\partial y}\right) = \frac{1}{Sc}\left(\frac{\partial^2 C}{\partial x^2} + \frac{\partial^2 C}{\partial y^2}\right). \tag{4.4}$$

In the above equations, $Gr = (\Delta\rho/\bar{\rho})(g/\omega^{3/2}\nu^{1/2})$ is a Grashof number based on the 'equivalent amplitude', g. All the other symbols have their usual meanings which are given in § 2. The initial conditions, the boundary conditions, and the solution procedure are also the same as described § 2. In this paper, we deal only with rational values of r for which T^* is chosen as an integer multiple of the larger of the two time periods of the individual components which constitute the modulation, $2\,\pi$ and $2\,\pi/r$. In this case, the equivalent amplitude, g, is given by the expression, $g = a\sqrt{1+\epsilon^2}$.

The reference values of the eight parameters governing the problem are as follows. We fix $Sc = 1$, $A = 0.2$, $l = 1000$, $\delta = 10$ as in the case for stochastic modulation, and ϕ is fixed at $\pi/4$. Gr was varied from 1 to 15. The amplitude of the secondary

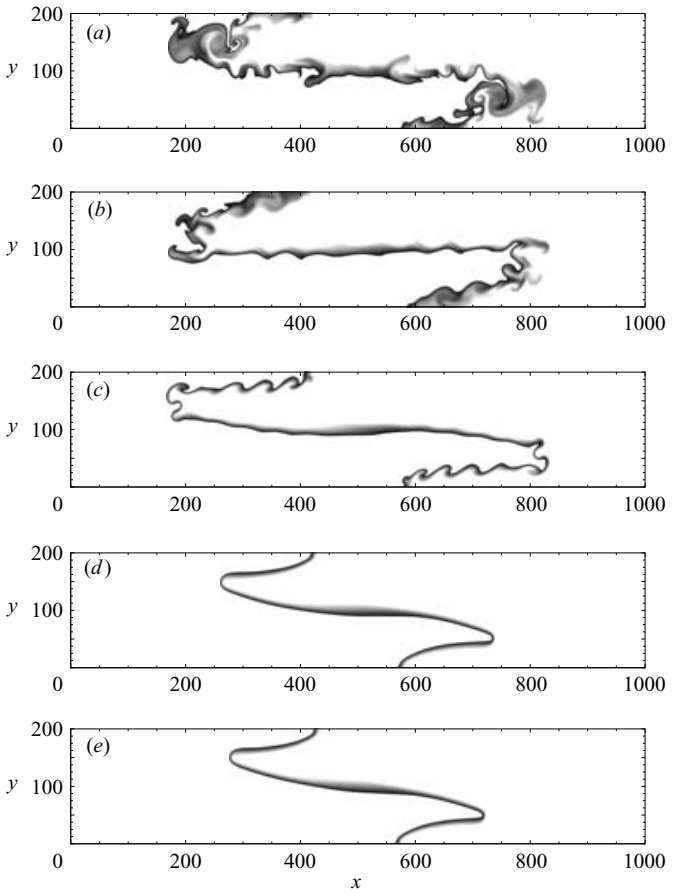

FIGURE 14. The concentration fields for $Gr = 20$ and $r = 2$ after $t = 10$ periods. (*a*) $\epsilon = 0$ – both KH and RT, (*b*) $\epsilon = 0.5$ – KH only, (*c*) $\epsilon = 1.0$ – KH only, (*d*) $\epsilon = 10$ – smooth gravity current. No instability (*e*) $\epsilon = 100$ – smooth gravity current.

component, ϵ, is varied from 0 to 100 and the frequency ratio, r, is varied from 0.2 to 2.0. We will mainly focus on the effects of varying r, ϵ and Gr.

In figure 14, we present the concentration fields for $Gr = 20$ and $r = 2.0$ for several values of ϵ. We point out that for the case of single-frequency modulation, we observed both KH and RT instabilities at this particular value of Gr. For $\epsilon = 0$, we recover this regime. As ϵ is increased, we note that the flow becomes less disordered, i.e. for higher values of ϵ, we observe only KH instability and for even higher ϵ, we do not observe any instabilities, and obtain a smooth gravity current instead. Thus we see that for $r > 1$, increasing the magnitude of the secondary component ϵ makes the flow less disordered. This is because as ϵ is increased, the amplitude of the secondary (in this case larger) frequency component increases, and we have observed in Part 1 that higher-frequency modulation tends to make the flow less disordered.

We observe the reverse trend when $r < 1$. In figure 15, we show the concentration fields for $r = 0.25$ and $Gr = 6$ for various values of ϵ. As can be seen, the flow becomes more disordered when the magnitude of the secondary component is increased. There are several interesting features in this figure. First, we note that when the modulation includes a secondary component, the instabilities are observed at much smaller Gr.

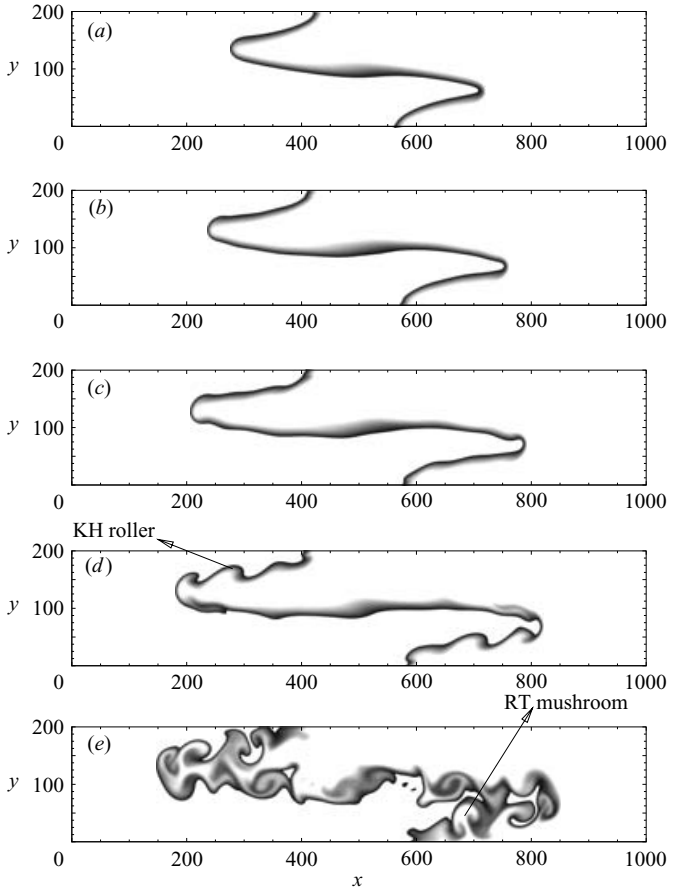

FIGURE 15. The concentration fields for $Gr = 6$ and $r = 0.25$ after $t = 19.25$ periods. (a) $\epsilon = 0$ – smooth gravity current, (b) $\epsilon = 0.1$ – smooth gravity current, (c) $\epsilon = 0.175$ – KH only, (d) $\epsilon = 0.25$ – KH only, (e) $\epsilon = 0.4$ – both KH and RT.

(As mentioned earlier, when the modulation has only a single component, the critical Gr at which we first observe RT instability is 18.) Secondly, for any Gr, we note that there is a critical value of ϵ for there to be significant deviation from the single-frequency modulation ($\epsilon = 0$) case, i.e. for instabilities to first occur. This point is clearly illustrated in figure 16, wherein we plot the critical ϵ for the occurrence of KH and RT instabilities as a function of r. This curve is valid only for $Gr = 6$. Naturally, we expect the curves to be different for different Gr. As can be seen, the ϵ_c are smaller for smaller r, because smaller frequencies are more effective at exciting instabilities. In figure 17, we present the concentration fields for different Gr for fixed r and ϵ. As expected, the flow becomes more disordered as Gr is increased.

As stated earlier, our primary motivation in analysing multiple-frequency modulation is to understand the results for stochastic modulation, specifically the non-monotonicity in mixed volume, based on our understanding of the results for this relatively simpler case. Since, stochastic modulation with non-zero modulation will include frequencies that are smaller and larger than the characteristic frequency, we consider the following three-frequency gravity modulation

$$g(t) = a(\cos(\omega t + \phi) + \epsilon_1 \cos(r_1 \omega t + \phi) + \epsilon_2 \cos(r_2 \omega t + \phi)).$$

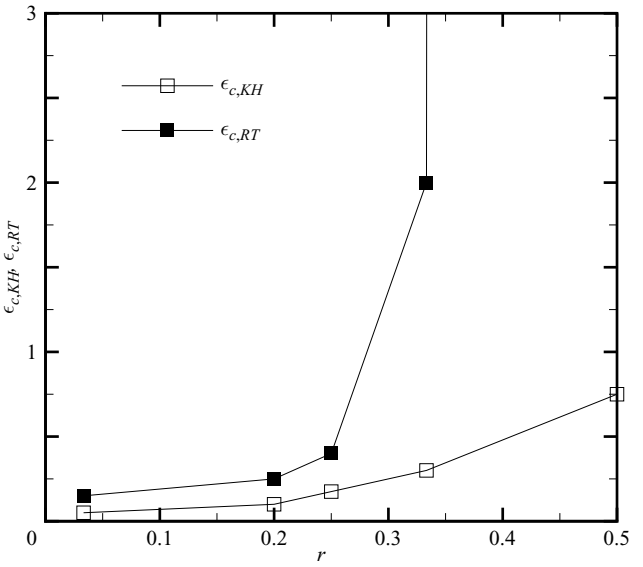

FIGURE 16. The variation of the critical values of ϵ for KH and RT instabilities, with r, for $Gr = 6$. For $r = 0.5$ we do not observe RT in the parameter range considered here.

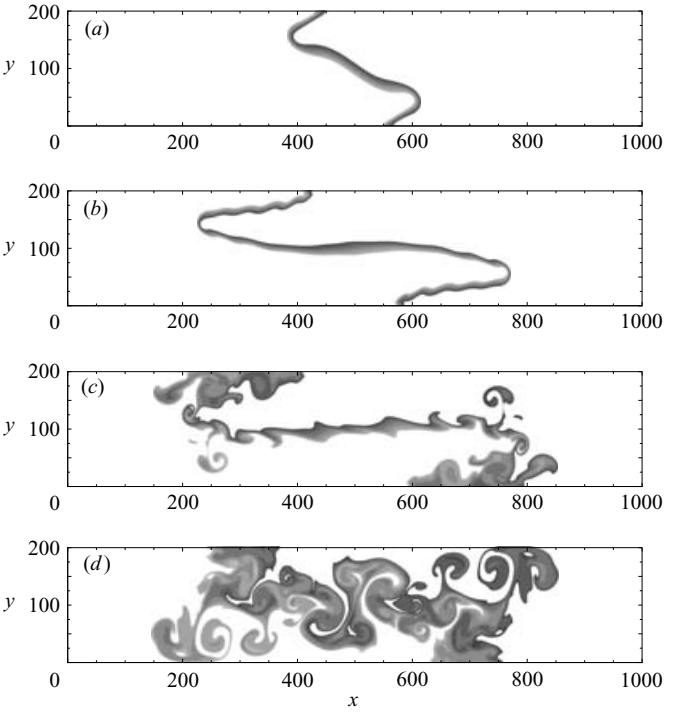

FIGURE 17. The concentration fields for different Gr after 13 periods for $r = 0.5$ and $\epsilon = 1$. (*a*) $Gr = 2$, (*b*) $Gr = 6$, (*c*) $Gr = 10$, (*d*) $Gr = 14$.

For reasons explained above, we take $r_1 < 1$ and $r_2 > 1$ and for simplicity, we take $\epsilon_1 = \epsilon_2 = \epsilon$. The non-dimensionalization scheme is the same as in the case for the two-frequency modulation. We have previously noted that when the secondary frequency

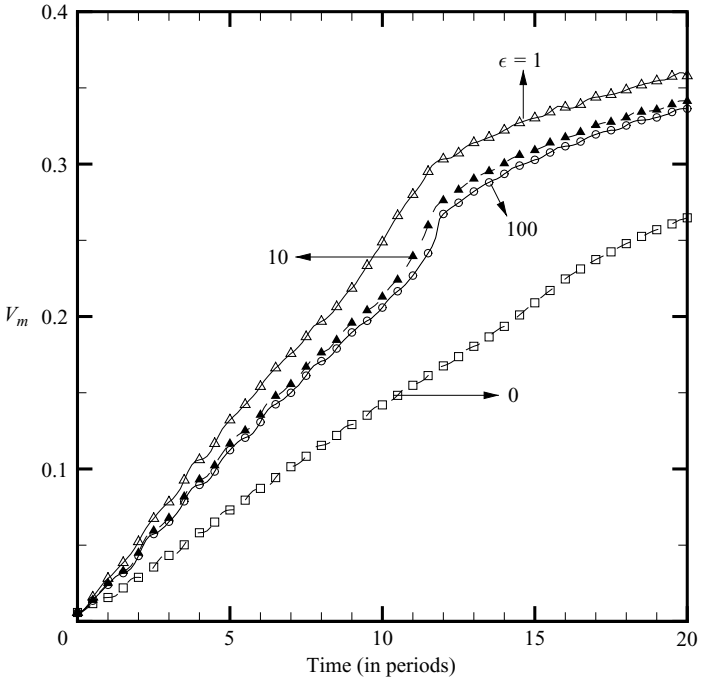

FIGURE 18. The variation of the fractional mixed volume, V_m *vs.* t for different ϵ for three-frequency modulation with $Gr = 6$, $r_1 = 0.25$ and $r_2 = 1.75$.

is smaller than the characteristic frequency, increasing the amplitude of the secondary modulation leads to a more disordered flow, whereas the reverse trend happens when the secondary frequency is larger than the characteristic frequency. Thus, for a three-frequency modulation which includes frequencies that are smaller and larger than the characteristic frequency, we expect a non-monotonic progression of the mixed volumes as ϵ is increased. This is indicated by figure 18, where we plot the fractional mixed volume, V_m with time, for various values of ϵ, and find that at any given time, the mixed volume for $\epsilon = 1$ is greater than that for $\epsilon = 0$ or $\epsilon = 100$, suggesting that the mixed volume varies non-monotonically with the amplitude of the secondary components. The same conclusion can also be drawn from figure 19, where we plot the individual concentration fields for different values of ϵ for $Gr = 6$. We can readily extend this result to the case of stochastic modulation which contains multiple frequencies, both smaller and larger than the characteristic frequency, whose amplitudes depend on λ. Thus as λ is varied, the amplitudes of the individual frequency components vary, and hence, as suggested by our simple three-frequency model, the mixed volume also varies non-monotonically.

5. Summary

We have investigated the physical mechanisms by which zero-mean stochastic gravity modulation affects the mixing of two miscible fluids which are initially separated by a thin vertical diffusion layer. The probability distribution function associated with the gravity modulation is Gaussian and the autocorrelation function is an exponentially damped cosine, given by $\langle g(t)g(t+\tau)\rangle / \langle g^2(t)\rangle = \mathrm{e}^{-\lambda\tau}\cos(\omega\tau)$. The gravity power spectrum is a Lorentzian with peak at ω and width λ. We define our

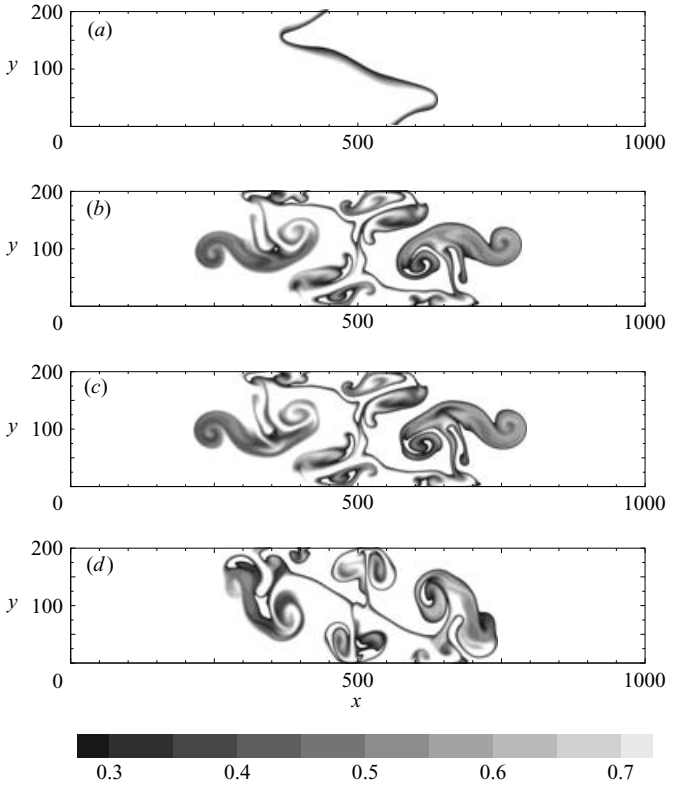

FIGURE 19. The individual concentration fields for different values of ϵ for three-frequency modulation with $Gr = 6$, $r_1 = 0.25$ and $r_2 = 1.75$, $\phi = \pi/4$ after 20 periods. (*a*) $\epsilon = 0$, (*b*) $\epsilon = 1$, (*c*) $\epsilon = 10$, (*b*) $\epsilon = 100$.

characteristic time scale based on the reciprocal of ω. We note that $\lambda = 0$ corresponds to monochromatic (harmonic) gravity modulation, small to moderate values of λ correspond to narrow-band modulation, and large values of λ correspond to broadband modulation. We invoke the Boussinesq approximation, solve the resulting equations numerically, and observe the evolution of the interface. The problem is governed by six parameters: the Grashof number, Gr; the Schmidt number, Sc; the correlation exponent, λ; the aspect ratio of the domain, A; the non-dimensional length of the domain, l; and the steepness of the initial concentration profile, δ.

In contrast to the case of harmonic modulation, which we considered in Part 1, we found that for narrow-band stochastic modulation with $\lambda = 1$, Kelvin–Helmholtz and Rayleigh–Taylor instabilities occur on the mixing front for a much smaller equivalent $Gr = 0.3$, which was the smallest Gr that we considered. Consequently, for any given Gr, the concentration field was more disordered and the fractional mixed volume was found to be much larger for the case of narrow-band modulation than for harmonic modulation. The individual realizations of the concentration field which exhibited higher mixing were characterized by the presence of large vortices, which are formed at the centre of the domain, owing to the merging of smaller rollers. The various phases in the merging of vortices were identified. This merged vortex acts as a stirring mechanism, which brings packets of different concentrations close together, thus increasing the concentration gradient, so that viscous diffusion can smooth them.

We found that the mixed volume at any given time is larger for narrow-band modulation, followed by harmonic modulation, and the smallest for broadband (white noise) modulation. This non-monotonicity of the mixed volume with λ is explained on the basis of the competition between the effects of excitation of lower frequencies and the effects of the attendant reduction in the energy content at the dominant frequency. The value of the correlation coefficient, λ, at which the mixed volume is the largest was found to be independent of Gr.

In order to further investigate this non-monotonicity of the mixed volume, we considered the effects of two- and three-frequency modulations. We found that increasing the amplitude of a secondary component whose frequency is smaller than that of the primary component leads to the occurrence of KH and RT instabilities at smaller Gr than those observed in the case of single-frequency modulation, whereas the reverse trend was observed when the secondary frequency is larger than the primary frequency. The critical amplitude of the secondary component for excitation of these instabilities was found to increase with the secondary frequency, confirming that lower-frequency modulation is more effective at exciting instabilities. By considering a three-frequency modulation, where one of the frequencies is smaller than the characteristic frequency and the other larger, as a simple prototype of stochastic modulation, we have explained the non-monotonic variation in the mixed volume.

This work was supported by the Microgravity Science Program of NASA.

REFERENCES

Antar, B. N. 1977 Thermal instability of stochastically modulated flows. *Phys. Fluids* **20**, 1785–1787.

Benjamin, T. B. & Ursell, F. 1954 The stability of the plane free surface of a liquid in vertical surface motion. *Proc. R. Soc. Lond.* A, 505–515.

Cerretelli, C. & Williamson, C. H. K. 2003 The physical mechanism for vortex merging. *J. Fluid Mech.* **475**, 41–77.

Drolet, F. & Viñals, J. 1997 Onset of oscillatory instabilites under stochastic modulation. *Phys. Rev.* E **56**, 2649–2657.

Duval, W. M. B. & Jacqmin, D. 1990 Interfacial dynamics of two fluids under an oscillating gravitational field. *AIAA Paper* 28-11.

Gresho, P. M. & Sani, R. L. 1970 The effects of gravity modulation on the stability of a fluid layer. *J. Fluid Mech.* **40**, 783–806.

Horsthemke, W. & Lefever, R. 1984 *Noise-Induced Transitions*. Springer.

Jhaveri, B. & Homsy, G. M. 1980 Randomly forced Rayleigh–Bénard convection. *J. Fluid Mech.* **98**, 329–348.

Jules, K., Hrovat, K., Kelly, E., McPherson, K. & Reckart, T. 2002 International space station increment-2 microgravity environment summary report. *NASA TM* 211335.

Meunier, P., Le Dizès, S. & Leweke, T. 2005 Physics of vortex merging. *C. R. Phys.* **6**, 431–450.

Siddavaram, V. K. & Homsy, G. M. 2006 The effects of gravity modulation on fluid mixing. Part 1. Harmonic modulation. *J. Fluid Mech.* **562**, 445–475.

Thomson, J., Casademunt, J. & Viñals, J. 1995 Cavity flow induced by a fluctuating acceleration field. *Phys. Fluids* **7**, 292–301.

Thomson, J., Casademunt, J., Drolet, F. & Viñals, J. 1997 Coarsening of solid–liquid mixtures in a random acceleration field. *Phys. Fluids* **9**, 1336–1343.

Winant, C. D. & Browand, F. K. 1974 Vortex pairing: the mechanism of turbulent mixing-layer growth at moderate Reynolds number. *J. Fluid Mech.* **63**, 237–255.

Zhang, W., Casademunt, J. & Viñals, J. 1993 Study of the parametric oscillator driven by narrow-band noise to model the response of a fluid surface to time-dependent accelerations. *Phys. Fluids* A **5**(12), 3147–3161.